Morphology, swimming performance and propulsive mode of six co-occurring hydromedusae

Sean P. Colin[1],* and John H. Costello[2]

[1]*Department of Marine Sciences, University of Connecticut, 1084 Shennecossett Road, Groton, CT 06340, USA* and
[2]*Biology Department, Providence College, Providence, RI 02918-0001, USA*

*e-mail: sean.colin@uconn.edu

Summary

Jet propulsion, based on examples from the Hydrozoa, has served as a valuable model for swimming by medusae. However, cnidarian medusae span several taxonomic classes (collectively known as the Medusazoa) and represent a diverse array of morphologies and swimming styles. Does one mode of propulsion appropriately describe swimming by all medusae? This study examined a group of co-occurring hydromedusae collected from the waters of Friday Harbor, WA, USA, to investigate relationships between swimming performance and underlying mechanisms of thrust production. The six species examined encompassed a wide range of bell morphologies and swimming habits. Swimming performance (measured as swimming acceleration and velocity) varied widely among the species and was positively correlated with bell streamlining (measured as bell fineness ratio) and velar structure development (measured as velar aperture ratio). Calculated thrust production due to jet propulsion adequately explained acceleration patterns of prolate medusae (*Aglantha* *digitale*, *Sarsia* sp. and *Proboscidactyla flavicirrata*) possessing well-developed velums. However, acceleration patterns of oblate medusae (*Aequorea victoria*, *Mitrocoma cellularia* and *Phialidium gregarium*) that have less developed velums were poorly described by jet thrust production. An examination of the wakes behind swimming medusae indicated that, in contrast to the clearly defined jet structures produced by prolate species, oblate medusae did not produce defined jets but instead produced prominent vortices at the bell margins. These vortices are consistent with a predominantly drag-based, rowing mode of propulsion by the oblate species. These patterns of propulsive mechanics and swimming performance relate to the role played by swimming in the foraging ecology of each medusa. These patterns appear to extend beyond hydromedusae and thus have important implications for other members of the Medusazoa.

Key words: Medusazoa, foraging, drag, shape, function, kinematics, wake structure, feeding, jet propulsion, jellyfish, swimming.

Introduction

Jet propulsion has commonly been described as the principal thrust-generating mechanism underlying swimming by planktonic medusae (Brusca and Brusca, 1990; Denny, 1993; Vogel, 1994). This view has been supported by detailed examinations of swimming by several species of hydromedusae (Gladfelter, 1972, 1973; DeMont and Gosline, 1988a,b,c; Daniel, 1983, 1985, 1995) and siphonophores (Bone and Trueman, 1982). Widespread acceptance of this view has led to its generalization, with the result that even scyphozoan medusae, which are morphologically quite different from their hydromedusan relatives, have also been described as jet-propelled swimmers (Larson, 1987; Costello and Colin, 1994, 1995).

However, the accepted view that jet propulsion is the principal thrust mechanism for all medusae deserves examination because medusae comprise a diverse assemblage of species and morphologies adapted to living in a variety of marine, and even some freshwater, habitats. In addition, the swimming patterns of medusae vary widely (Mills, 1981a; Larson et al., 1992; Strand and Hamner, 1988; Costello and Colin, 1995; Costello et al., 1998). For some medusae, swimming affects feeding because swimming and prey capture are simultaneous, interrelated processes (Costello, 1992; Costello and Colin, 1994, 1995; Ford et al., 1997; D'Ambra et al., 2002). For others, prey capture occurs only in the absence of swimming (Madin, 1988). Consequently, because swimming appears to have different roles during foraging for different medusae, mechanisms of medusan swimming have significant ecological ramifications. The application of a single, uniform model of medusan swimming to all medusae may therefore lead to inappropriate conclusions about medusan foraging. Hence, it is important to examine the suitability of the jet-propelled swimming model for all medusae.

We addressed this issue using a group of seasonally co-occurring hydromedusae found in the waters surrounding Friday Harbor Laboratory, WA, USA. These medusae (Fig. 1)
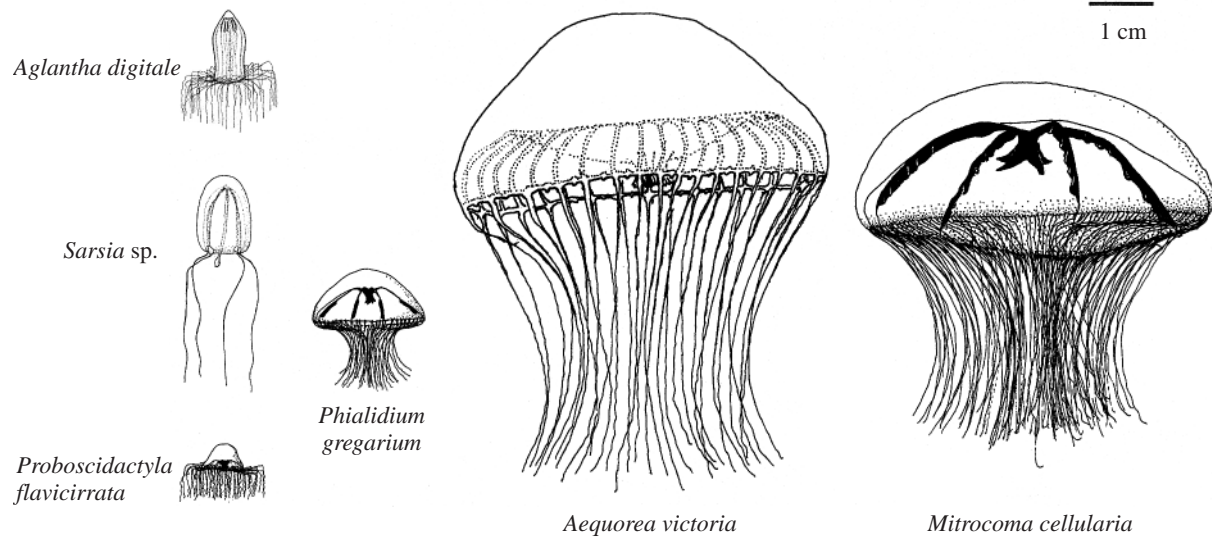
Fig. 1. Representative examples of the hydromedusae from Friday Harbor, WA, USA, selected for comparative study. Medusae are shown with their bells relaxed and are drawn to scale among species. *Aequorea victoria* and *Mitrocoma cellularia* can grow to be twice as large as depicted.

include a variety of bell morphologies ranging from small, prolate to large, oblate bells. Swimming behavior (Mills, 1981a), prey selection (Mills, 1995) and seasonal distribution patterns (Mills, 1981b) have been described for these species. Our intention was to use this group to compare three aspects of hydromedusan swimming: (i) patterns of swimming performance, particularly in relation to bell form and function, (ii) the adequacy of jet propulsion to explain observed swimming performance patterns and (iii) thrust-generating mechanisms. Our intention in using these complementary approaches was to achieve an integrated view of key traits influencing medusan swimming mechanisms.

Materials and methods

Specimen collection and microvideography

Individual hydromedusae of the six species studied (Fig. 1), *Aglantha digitale*, *Sarsia* sp., *Proboscidactyla flavicirrata*, *Phialidium gregarium*, *Aequorea victoria* and *Mitrocoma cellularia*, were collected by hand from surface waters adjoining the dock off Friday Harbor Laboratories, San Juan Island, Washington, USA, during June–August in 1992–1994. Medusae were carefully transported within seawater-filled containers to the laboratory and placed into vessels with sea water. Video recordings of swimming medusae were made within 48 h of collection.

Video recordings (SVHS) were made following the methods of Costello and Colin (1994). Medusan swimming and particle flow were recorded using a backlit optical system. Recordings were labeled with a field-counter to provide temporal data. Spatial characteristics of the optical field were determined from scale bars periodically included in the original recordings. Morphological measurements such as bell diameter and length were thus made directly from video recordings calibrated with

scale bars. VHS recordings were used to detail movements of medusae and their surrounding fluids.

Morphological traits of medusae

Alterations in bell shape were quantified by the fineness ratio, F:

$$F = h/d, \qquad (1)$$

where h is bell height and d is bell diameter. Instantaneous fineness ratio, F_i, represents the fineness ratio at the midpoint of an interval used for measurement of medusa velocity. F_i was determined to quantify variations in bell morphology during the pulsation cycle. The fineness ratio of the bell at rest in its uncontracted state corresponds closely to the minimum F_i value, whereas maximum F_i corresponds to full bell contraction.

A second morphological variable, the velar aperture area ratio, compared the area of the velar aperture with the total area encompassed by the velum during bell relaxation. For most species, the maximum bell diameter occurred at the bell margin, adjacent to the base of the velum. Velar aperture ratio was used as an index of the degree to which the fluid jet leaving the subumbrellar was constricted during its passage through the velar aperture during bell contraction. Measurements were made from video recordings of medusae at rest because of the difficulty of imaging the velum during bell contraction. The bell diameter (d) and the diameter of the velar aperture (v) were measured for 7–10 medusae of each species. Assuming that the velar aperture and the bell were circular in cross section, the ratio of their areas, the non-dimensional velar aperture ratio, R_v, can be simplified to:

$$R_v = v^2/d^2. \qquad (2)$$

A low velar aperture ratio reflects a narrow velar aperture relative to the entire velar area. Conversely, a high velar

aperture ratio reflects a large velar aperture relative to the area of the entire velum.

Kinematic analysis of swimming

All data were collected from video recordings of normally swimming medusae. Rapid escape response swimming sequences of *Aglantha digitale* were not used because of the unique nature of this type of swimming (Donaldson et al., 1980). One swimming sequence for each of three replicate individuals was analyzed for each species of hydromedusa. Each swimming sequence consisted of 2–6 complete bell pulsations.

Medusa motion was measured from sequential changes in position (x) of the anteriormost point of the exumbrellar surface over 0.05–0.08 s intervals (t). The subscript i is used in equations to denote instantaneous measurements and parameters calculated from instantaneous measurements. Motion only within the two-dimensional viewing field was ensured by using a sequence in which bell orientation was level and the medusa swam from bottom to top of the viewing field.

The velocity (u) at time i was calculated over the time interval t as an average:

$$u_i = \frac{x_{i+1} - x_{i-1}}{2t}. \tag{3}$$

Instantaneous acceleration (A_o) was calculated as:

$$A_{o,i} = \frac{x_{i+1} + x_{i-1} - 2x_i}{t^2}. \tag{4}$$

Reynolds number (Re) was calculated as:

$$Re_i = d_i u_i / \nu, \tag{5}$$

where d_i and u_i are the instantaneous medusan diameter and velocity, respectively, and ν is the kinematic viscosity of sea water.

Statistical analysis utilized analysis of variance (ANOVA) tests (Statistica, Statsoft Inc.). Individual comparisons between species were based on Tukey's honest significant difference (HSD) test. Linear relationships between two variables were quantified using linear regression, and the strength of a relationship is reported as the coefficient of determination (r^2) and the probability that the relationship was significant.

Model of jet propulsion

Morphometric and kinematic data were combined to model jet thrust production for all medusae. The net force available to accelerate an animal was defined as thrust minus the combined effect of its weight and drag (Denny, 1993). Accordingly, we used estimates of jet thrust (T) and drag (D) to calculate an instantaneous modeled acceleration (A_m) due to jet thrust such that:

$$A_{m,i} = [T_i - (D_i + W)]/E_i. \tag{6}$$

Medusan weight (W) was neglected since the medusae were essentially neutrally buoyant (Denton and Shaw, 1961). Estimates of T, D and effective mass (E) were based on the kinematic profiles (see Figs 2, 3) and morphological measurements determined from video recordings of swimming medusae. Calculations followed the methods of Daniel (1983, 1985). T was determined as the product of the change in mass of the object per unit time (dm/dt) and velocity of the fluid (j), both resulting from fluid being ejected away from the object. The change in mass per unit time is estimated by:

$$dm/dt = \rho \, dV_{s,i}/dt, \tag{7}$$

where ρ is the density of sea water at 25 °C ($\rho = 1.024$ g cm^{-3}) and $V_{s,i}$ is the instantaneous subumbrellar volume. The subumbrellar volume was estimated throughout the swim cycle using the equation for the volume of a hemi-ellipsoid ($\frac{1}{3}\pi d l^2$, where l is the height of the subumbrellar cavity) using medusan cavity dimensions. The jet velocity (j) was estimated as:

$$j_i = (1/A_v)(dV_{s,i}/dt), \tag{8}$$

where A_v is the orifice area. The velar aperture area was measured from medusae at rest (see equation 2) because Gladfelter (1973) found that this value remained constant throughout the swim cycle. Thrust is the product of dm/dt (equation 7) and the velocity (equation 8) of the fluid ejected:

$$T_i = (\rho/A_v)(dV_{s,i}/dt)^2. \tag{9}$$

Drag (D) was calculated using the equation:

$$D_i = \tfrac{1}{2}\rho u_i^2 S_i C_{D,i}, \tag{10}$$

where u_i is the instantaneous velocity of the medusa (equation 3) and S_i is the instantaneous projected surface area. The surface area was calculated using the equation for the surface area of a hemi-ellipsoid, $\pi h_i d_i/4$. The drag coefficient C_D was calculated as a function of the Reynolds number from the relationship:

$$C_{D,i} = 24/Re_i^n \tag{11}$$

provided by Daniel (1983), where $n=1$ for Reynolds numbers less than 1 and $n=0.7$ for Reynolds numbers between 1 and 500. The mass of fluid surrounding a medusa that is accelerated with the medusa, termed the added mass, was calculated as the product of the medusa's mass and the added-mass coefficient (α) (Daniel, 1984, 1985):

$$\alpha_i = 0.5 d_i / h_i^{1.4}. \tag{12}$$

Thus, the effective mass (E) was the sum of the medusa's mass and its added mass:

$$E_i = V_{b,i}\rho[1 + (0.5 d_i/h_i)^{1.4}]. \tag{13}$$

$V_{b,i}$ is the volume of the medusa's bell based on the equations for a hemi-ellipsoid (Colin and Costello, 1996).

Flow field description

Quantitative description of the fluid motions surrounding the medusae utilized particles tracked in the fluid surrounding the bell. The particles used for tracking were naturally occurring phytoplankton cells. Particle tracks were collected during the period of maximum medusan acceleration. However, the

duration of the power stroke varied between different species of medusae and affected the relative timing of particle data collection. Measurement of particles began three video fields (0.05 s) before maximum contraction for oblate medusae but, because of the shorter contraction times, only one field before maximum contraction for prolate species. These methods are essentially the same as those of Costello and Colin (1994, 1995). Flow-field images were taken while the camera was stationary and the medusa swam through the field of view. The flow field was constructed from several pulsation cycles because no single cycle contained enough appropriately located and focused particles to describe the entire flow field. We measured the flow field by superimposing an x,y grid on a video sequence of a free-swimming medusa. Since the swimming medusa's position changed, the x,y grid was positioned relative to the medusa's bell. Therefore, all particle velocities were measured with respect to the medusa's bell. Particle velocities were determined on the basis of the changes in their positions over a 0.05 s interval. The position of the particle throughout the interval was traced, thus allowing us to draw the paths of particles not travelling in a straight line.
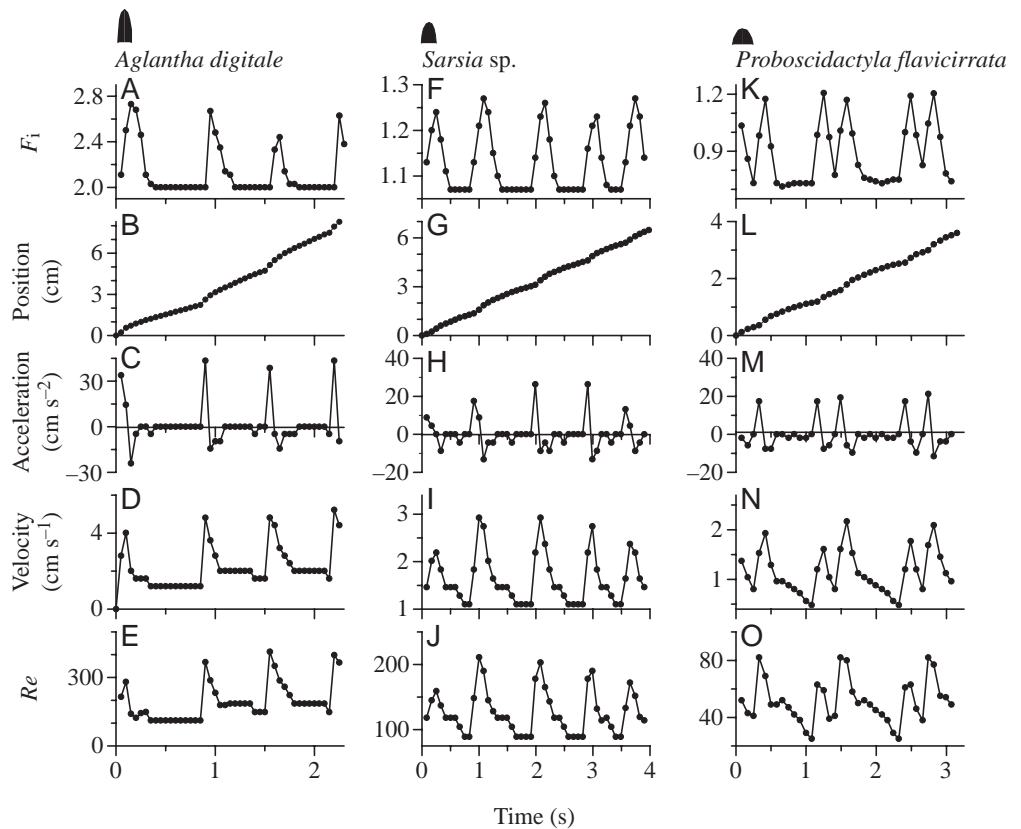

Fig. 2. Representative kinematic profiles of individual prolate medusae. All graphs in the left-hand column refer to *Aglantha digitale* (2.03 cm height, 0.83 cm diameter), in the middle column to *Sarsia* sp. (0.91 cm height, 0.85 cm diameter) and in the right-hand column to *Proboscidactyla flavicirrata* (0.40 cm height, 0.56 cm diameter). Note the differences in the x and y axes. Re, Reynolds number; F_i, instantaneous fineness ratio.

Results

Kinematic patterns

Cyclic bell pulsation, indicated by changes in the fineness ratio, F_i (Figs 2A,F,K, 3A,F,K), resulted in positional changes of medusae as they swam through the water (Figs 2B,G,L, 3B,G,L). Maximum accelerations for all species immediately preceded maximum bell contraction (Figs 2C,H,M, 3C,H,M) and typically peaked prior to maximum medusan velocities (Figs 2D,I,N, 3D,I,N). Reynolds numbers were closely related to medusan velocities and typically peaked at the end of bell contraction (indicated by peak F_i) and the beginning of bell relaxation (Figs 2E,J,O, 3E,J,O).

Swimming performance and bell morphology

The kinematic data (Figs 2, 3) for replicates of each species were combined to examine underlying patterns of hydromedusan morphology and function. Nominally on the basis of bell shape, but also of kinematic patterns (Figs 2, 3), medusan species were grouped as 'prolate' (*Aglantha digitale*, *Sarsia* sp. and *Proboscidactyla flavicirrata*) or 'oblate' (*Aequorea victoria*, *Mitrocoma cellularia* and *Phialidium gregarium*) forms. The oblate species all possessed flatter bells (fineness ratio less than 0.5) than the prolate medusae (fineness ratio greater than 0.5). In addition, a number of other traits delineated the two categories of medusae. Oblate species did not differ in their velar aperture ratios, maximum accelerations or maximum velocities (ANOVA, $P>0.05$, Fig. 4C,D,E). Within the prolate species, bell contraction duration did not vary significantly (ANOVA, $P=0.224$) among species. Velar aperture ratios for *Sarsia* sp. and *Proboscidactyla flavicirrata* were not significantly different (Tukey's HSD, $P=0.693$), but the velar aperture ratio was significantly lower (Tukey's HSD, $P<0.001$) for *Aglantha digitale* than for the other two prolate species. These groupings, although reflecting morphological and functional traits, were used for comparative generalizations and were not intended to imply that all species of either group were uniform in their swimming patterns.

A comparison between the oblate and prolate medusae reveals, however, that the swimming performance of the two groups varied. Bell contraction by the prolate group was more rapid (ANOVA, *P*<0.002; Fig. 4B,H) and velar aperture areas were proportionately smaller in the prolate (ANOVA, *P*<0.001; Fig. 4C,I) than the oblate group. As a result, prolate medusae achieved higher accelerations than oblate genera (Fig. 4D,J). Although all the prolate species accelerated more rapidly than the oblate forms, the differences in acceleration were only significant for *Aglantha digitale* (Tukey's HSD, *P*<0.001). With the exception of *Proboscidactyla flavicirrata*, prolate species reached higher maximum velocities (Tukey's HSD *P*<0.001 for all comparisons of both *Sarsia* sp. and *Aglantha digitale* with other species; Fig. 4K) than did oblate species.

Peak flows around all the swimming medusae, except *Proboscidactyla flavicirrata*, were dominated by inertial forces (*Re*>100; Fig. 4F,L). *Re* was influenced by two major patterns. First, peak *Re* values increased significantly with bell diameter (linear regression, r^2=0.79, *P*<0.001; Fig. 4F). Second, the higher velocities of rapidly swimming *Aglantha digitale* were reflected in high *Re* values and formed the basis of a secondary trend relating increased *Re* value to increases in bell fineness. This pattern was significant (linear regression, r^2=0.90, *P*<0.001) when oblate species were excluded from consideration.

Model of jet propulsion

The utility of jet-based swimming models for describing medusan swimming was tested by comparing peak accelerations derived from a model assuming solely jet propulsion (equation 6) with observed accelerations from swimming medusae. The modeled and observed accelerations would be most likely to diverge during periods of maximum acceleration. Consequently, these peak values were used to estimate the goodness of fit between modeled and observed accelerations during medusan swimming.

Accelerations, either modeled or observed, were not significantly different among individuals of a species (*N*=3; ANOVA, *P*>0.05). This high consistency within each species permitted comparisons of acceleration patterns among species.

A representative comparison of acceleration patterns for a prolate and an oblate species illustrates some of the patterns common to species of both groups (Fig. 5). *Sarsia* sp.
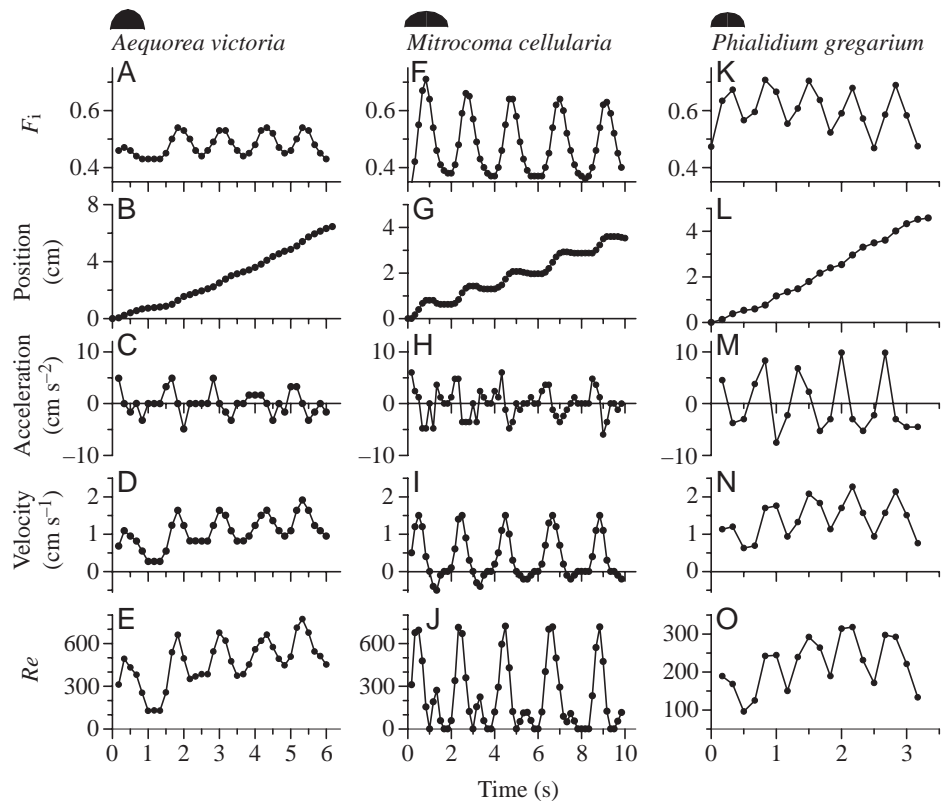

Fig. 3. Representative kinematic profiles of individual oblate medusae. All graphs in the left-hand column refer to *Aequorea victoria* (2.09 cm height, 5.00 cm diameter), in the middle column to *Mitrocoma cellularia* (2.03 cm height, 6.50 cm diameter) and the right-hand column to *Phialidium gregarium* (0.84 cm height, 2.14 cm diameter). Note the differences in the *x* and *y* axes. *Re*, Reynolds number; F_i, instantaneous fineness ratio.

accelerated rapidly in bursts between periods of gliding characterized by low values for both modeled and observed acceleration (Fig. 5A). In comparison, *Phialidium gregarium* swam with more even, sinusoidal variations in acceleration (Fig. 5B). Whereas modeled and observed peak accelerations were fairly similar for *Sarsia* sp. (ANOVA, *P*=0.42 for combined *Sarsia* sp. individuals), modeled peak accelerations were significantly lower than observed values for *Phialidium gregarium* (ANOVA, *P*<0.02 for combined *Phialidium gregarium* individuals). More generally, these patterns were representative of differences in accelerations between the prolate and oblate species (Fig. 6). Modeled peak accelerations were not significantly different from observed values for any of the prolate species (ANOVA, *P*≥0.1 for all prolate species), but modeled values were significantly lower than observed values for all the oblate species (ANOVA, *P*<0.0001 for both *Aequorea victoria* and *Mitrocoma cellularia*). Therefore, acceleration patterns calculated using a model that assumed solely jet propulsion adequately explained observed acceleration patterns for the prolate but not the oblate medusan species.

Fluid motions surrounding swimming medusae

Fluid flows, quantified by using particle paths, varied among
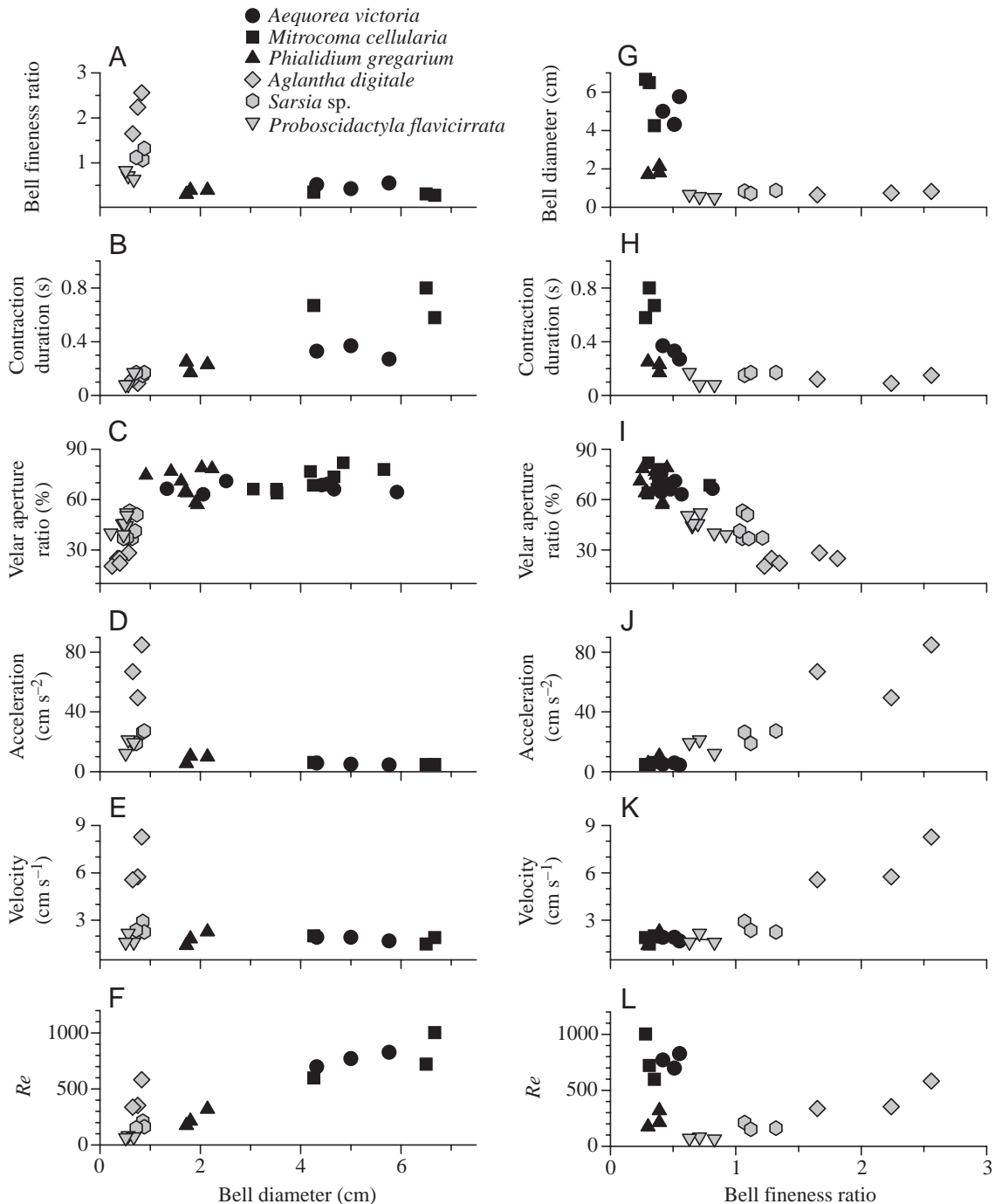
Fig. 4. Relationships between bell morphology and swimming performance for individuals representing six species of co-occurring hydromedusae from Friday Harbor, WA, USA. Performance variables (maximum velocity and maximum acceleration) and velar aperture ratios of individual medusae are described as a function of both bell diameter and fineness. Grey and black symbols denote prolate and oblate medusan forms, respectively. *Re*, Reynolds number.

medusae. Prolate species, *Aglantha digitale*, *Sarsia* sp. and *Proboscidactyla flavicirrata*, created strong jets during bell contraction. These species also contracted their tentacles while swimming. As a result, a strong jet component was evident in their wake (Fig. 7), with maximal flow velocities located directly behind the velar aperture. In contrast, the oblate medusae created substantially more diffuse jets (Fig. 7). Broad

vortices, shed at the bell margin during contraction, were pronounced for all oblate, but not prolate, medusae. These vortices traveled through the tentacles extended by all three oblate medusae during swimming (Fig. 7). As a result, prey suspended in the fluid adjacent to the bell margin were entrained and often observed to be carried into contact with the tentacles trailing in the medusa's wake.
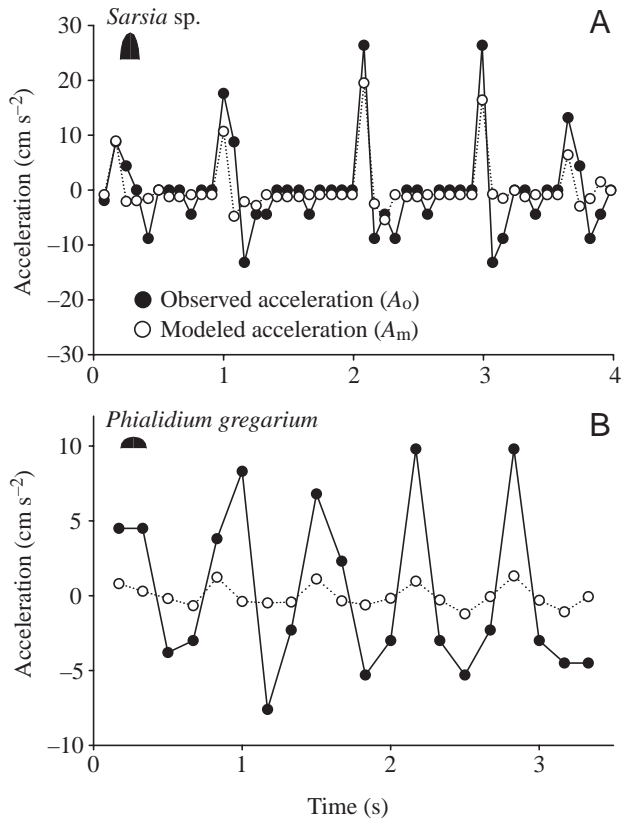
Fig. 5. Observed acceleration (A_o, filled symbols) and modeled acceleration (A_m, open symbols) from the force balance equation (equation 6) of *Sarsia* sp. (A) and *Phialidium gregarium* (B) during the swimming profiles illustrated in Figs 2 and 3.

Fig. 6. Means and standard deviations (N=3) of the maximum observed (A_o, open symbols) and modeled (A_m, filled symbols) accelerations achieved during each pulse of the swim cycle for the six species of hydromedusae studied. Asterisks designate a significant difference between A_m and A_o (ANOVA; *P<0.05).

Discussion

Relationships between bell form, function and swimming performance

The assemblage of medusae found in waters surrounding Friday Harbor, WA, USA, is characterized by diverse morphologies, swimming performance and swimming mechanics. However, this diversity is underlain by patterns that relate bell form and function during swimming. One of the most outstanding morphological features differentiating medusae, bell shape, has long been recognized as a key variable affecting swimming performance (Gladfelter, 1973; Daniel, 1983, 1985; Colin and Costello, 1996) and served as a first organizing parameter with which we characterized distinctions in swimming between medusan species.

Swimming performance, here defined as the ability of a medusa to translate its body through the surrounding fluid, was higher for the prolate hydromedusae (*Aglantha digitale*, *Sarsia* sp. and *Proboscidactyla flavicirrata*) than for the oblate hydromedusae (*Phialidium gregarium*, *Aequorea victoria* and *Mitrocoma cellularia*). Both velocity and acceleration (Figs 2, 3) profiles confirm that the oblate hydromedusae do not propel themselves through the water as well as do the prolate hydromedusae.

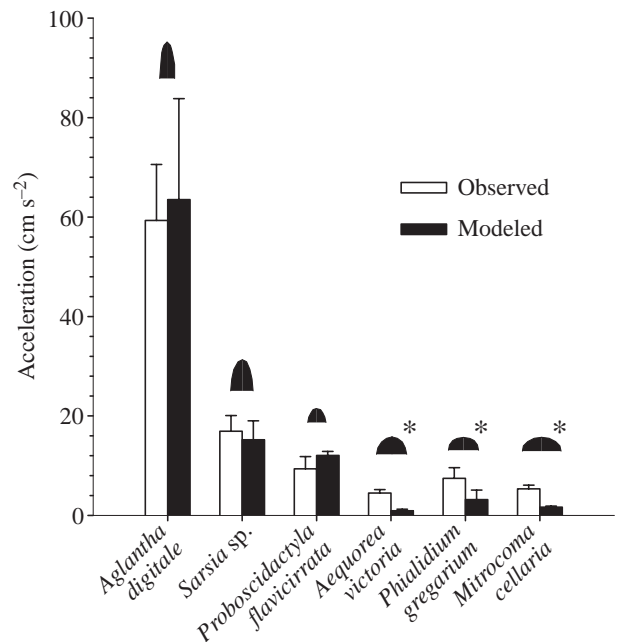The higher velocities and accelerations achieved by the prolate medusae can be explained mechanistically by relating their body form to the balance of forces in swimming. Swimming performance is optimized by maximizing thrust production while minimizing the forces that resist movement in a fluid. The velocity and the momentum flux of the fluid expelled from the medusa's subumbrellar cavity determine the amount of force produced during a pulse (Daniel, 1983; Vogel, 1994). By maximizing the rate of decrease in subumbrellar volume (i.e. rapid bell contraction) and minimizing the area through which water exits the subumbrellar cavity during bell contraction (i.e. low velar aperture ratio), medusae increase the velocity and momentum flux of the fluid jet. As a consequence, these same patterns maximize jet-dependent thrust production. The comparatively low bell contraction durations and velar aperture ratios of the prolate medusae (Fig. 4) result in relatively high jet thrust production. In turn, high rates of thrust production contribute to high acceleration rates and velocities. By comparison, the long contraction durations and larger velar aperture ratios of the more oblate medusae are not traits that optimize jet thrust production.

In addition to thrust production, swimming performance is dependent on the medusa's ability to reduce the forces that resist motion. The variables involved in determining the magnitude of these forces were described by Daniel (1983, 1985) and subsequently quantified by Colin and Costello (1996) for hydromedusae. The dominant forces acting on the swimming hydromedusae, based on the measured range of Re values (Fig. 4), are drag, the acceleration reaction and the force needed to overcome the inertia of the medusae. Streamlining

Aglantha digitale —   *Sarsia* sp. ——   *Proboscidactyla flavicirrata* ————

Aequorea victoria —   *Mitrocoma cellularia* —   *Phialidium gregarium* —
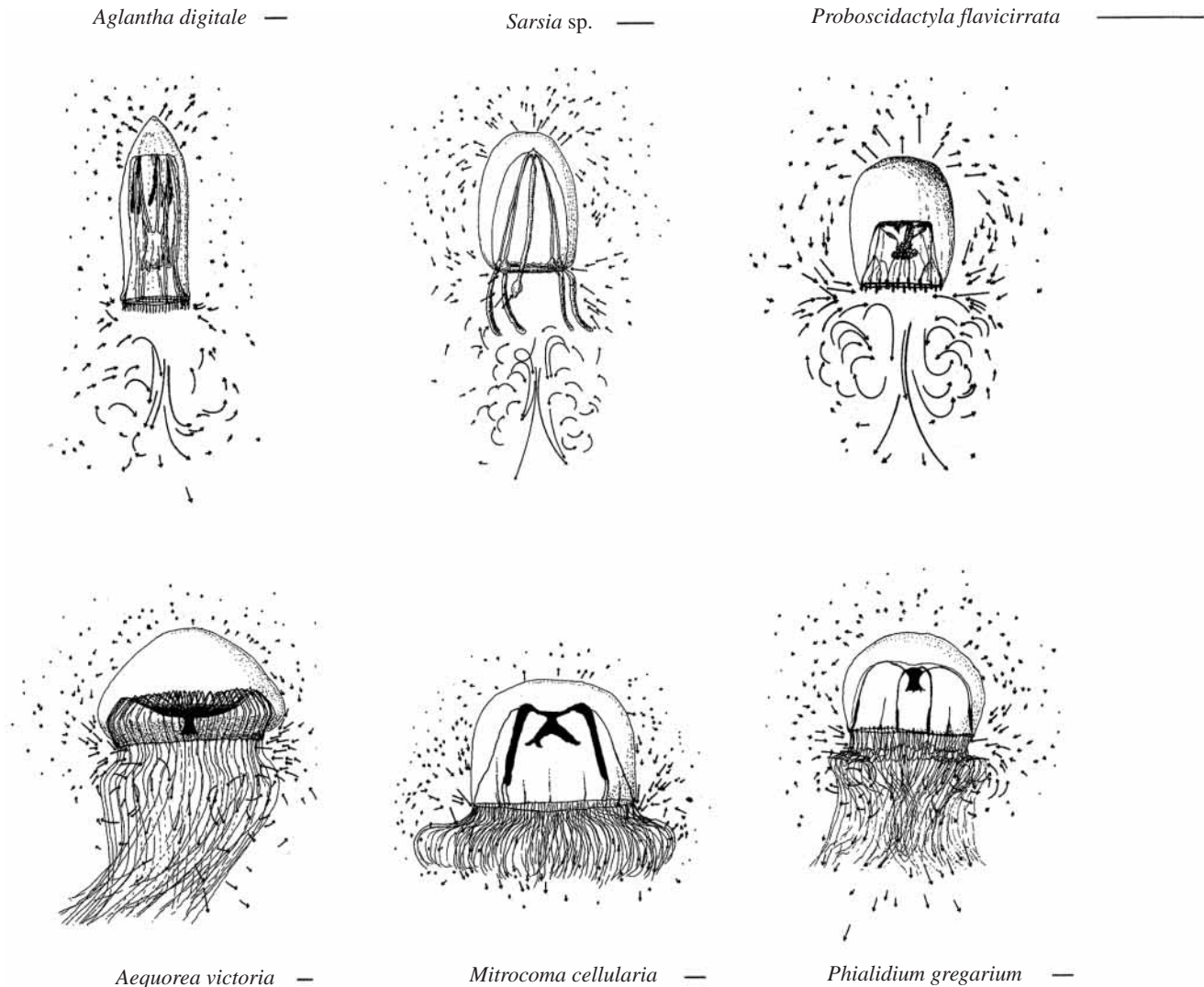
Fig. 7. Flow patterns around swimming hydromedusae. Arrows represent particle paths at the end of the effective phase of bell pulsation. Arrow lengths represent particle velocities. The bars to the right of each species' name are a scaling reference and represent a particle velocity of $3\,cm\,s^{-1}$. Medusae diameters (cm) were as follows: *Aglantha digitale*, 0.68; *Sarsia* sp., 0.8; *Proboscidactyla flavicirrata*, 0.54; *Aequorea victoria*, 4.32; *Mitrocoma cellularia*, 6.8; *Phialidium gregarium*, 2.2. Medusae are drawn at maximum contraction.

(higher fineness ratio) reduces drag. Therefore, the streamlined body forms of *Aglantha digitale* and *Sarsia* sp., and to a lesser extent *Proboscidactyla flavicirrata*, are able to contribute to their high swimming performance.

However, the influence of the acceleration reaction can be a major force resisting motion of organisms that periodically pulse, such as medusae, and therefore undergo frequent changes in their acceleration (Daniel, 1983, 1984, 1985). The amount of fluid that is accelerated along with the medusa, termed the added mass of the medusa, is estimated using a coefficient determined by bell shape. The added mass decreases in magnitude with increasing fineness ratio (Daniel, 1985). Therefore, the streamlined body forms of the prolate medusae reduce the acceleration reaction experienced during swimming (Colin and Costello, 1996). In addition, the acceleration reaction is directly related to the volume of the

medusa (Daniel, 1983). Thus, the reduced body size of the prolate medusae further reduces their acceleration reactions during swimming. The results of Colin and Costello (1996) support this by demonstrating that, despite its considerably higher acceleration, the acceleration reaction of *Aglantha digitale* was two orders of magnitude less than that of the comparatively larger oblate medusa *Aequorea victoria*. The small volume of the prolate medusae also reduced the initial force required to overcome inertia at the outset of swimming.

Taken together, the traits characterizing bell form and function – bell fineness ratio, bell size, velar aperture ratio and bell contraction rates – favor relatively high thrust production and low hydrodynamic resistance to forward motion for prolate medusae, whereas the same traits result in comparatively low thrust production and elevated hydrodynamic resistance for

oblate medusae. Within the medusae examined here, the traits affecting swimming performance appear to occur as a co-evolved suite of characteristics. For example, high bell fineness ratio, relatively small size, low velar aperture ratio and rapid bell contraction are most characteristic of medusae that are well suited for comparatively rapid swimming *via* jet propulsion. The terms we have used to group species – either prolate or oblate – nominally refer to bell fineness ratio but more realistically reflect the balance of the full suite of these characters. Thus, despite its intermediate bell shape, *Proboscidactyla flavicirrata* was included within the prolate group because it shared the other morphological and performance characteristics of the prolate medusae. Likewise, although *Phialidium gregarium* was smaller and some aspects of its swimming differ from those of larger oblate species such as *Aequoria victoria* (Ford and Costello, 2000), the oblate genera examined here tended to be similar in performance characteristics.

Thrust production mechanisms for medusan swimming

Swimming performance traits were a reflection of the importance of jet propulsion for thrust generation during medusan swimming. A comparison of peak accelerations calculated on the basis of the model of jet thrust production (A_m) with observed accelerations (A_o) indicated that, although jet propulsion provided sufficient thrust to explain the observed acceleration patterns of prolate medusae, it was unlikely that the oblate medusae we examined could rely exclusively upon jet propulsion as the primary source of their propulsive thrust (Fig. 6). In fact, jet thrust production accounted for only 21–43 % of the observed acceleration rates of the three oblate species, compared with 90–100 % for the prolate species. Therefore, we suggest that, although jet propulsion alone provides sufficient thrust for swimming prolate species, an alternative mechanism is necessary to describe swimming by oblate medusae.

Changes in the bell shape during bell contraction provide insight into mechanisms of thrust generation by swimming medusae. Bell contraction by prolate medusae (specifically *Aglantha digitale* and *Sarsia* sp.) occurs essentially evenly along the length of the bell. In contrast, bell contraction by oblate genera (*Aequorea victoria* and *Phialidium gregarium*) occurs primarily at the bell margin (Ford and Costello, 2000). The uniformly distributed bell contraction by prolate medusae produces pressure in the subumbrellar chamber and results in the expulsion of fluid through the velar aperture as a jet directed normal to the direction of bell contraction (Fig. 8A). In contrast, non-uniform bell contraction along the bells of oblate genera causes the region experiencing extensive contraction, the bell margin, to move relative to less actively contracting bell regions (Fig. 8B). As a result, movement at the bell margin of oblate medusae describes an arc which initially, during the period of maximum fluid acceleration, parallels the direction of medusan motion (Fig. 8B) and creates vortices adjacent to the bell margin. These flows adjacent to the bell margin are characterized by
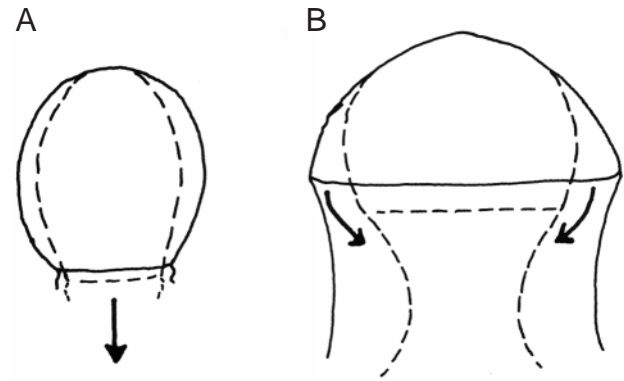

Fig. 8. Schematic diagram illustrating the change in bell shape during bell contraction of swimming prolate (A) (e.g. *Sarsia* sp.) and oblate (B) (e.g. *Phialidium gregarium*) medusae and the region of maximum flow (arrows) around each medusa. Bell shapes are based on the measured fineness ratios of each medusa at minimum and maximum contraction.

the highest velocities within the wakes of oblate medusae (Figs 7, 8B).

This type of bell movement and wake production pattern is more consistent with a rowing type of thrust production than with jet propulsion. In this case, the bell margin acts like a paddle as the medusa rows through the fluid. Accordingly, thrust may be generated by both the drag acting on the bell margin (drag-based propulsion) and the acceleration reaction associated with the bell margin. During drag-based propulsion, the rearward drag equals the forward thrust (Blake, 1981). When the velocity of the bell margin is greater than the velocity of the water movement adjacent to the margin, the movement of the bell will impart momentum to the surrounding fluid and create thrust (Lauder and Jayne, 1996). The thrust produced is proportional to the excess velocity of the appendage over the forward motion of the body to which it is attached (Blake, 1981). In addition, as a result of its added mass, the deceleration of the margin at the end of the power stroke accelerates the surrounding fluid, resulting in a net forward thrust (Daniel, 1984; Lauder and Jayne, 1996). Analysis of bell margin motion relative to overall body motion by oblate medusae is consistent with this type of rowing (Fig. 8) (Ford and Costello, 2000).

The relative contributions of jet and rowing propulsion to total thrust production reflect variations in bell form and function and vary among oblate medusan species. Although the flow-field patterns of oblate medusae indicate that maximum flows occurred near the bell margins, there was also evidence of jet production through the velar aperture. Therefore, although rowing may dominate thrust generation by oblate medusae, jetting does contribute to total thrust production, and the two mechanisms of thrust generation may act synergistically. The relative importance of either mechanism depends upon the morphology and contraction characteristics of a medusa's bell.

Propulsive mechanisms, flow patterns and foraging strategies

Propulsive mechanisms affect fluid flow around medusae in ways that are fundamentally important to medusan foraging strategies. As ambush predators, the prolate medusae spend most of their time sitting motionless with their tentacles extended to entangle actively swimming prey. These medusae swim primarily while escaping or repositioning themselves in the water column. Because their tentacles are typically retracted while swimming, feeding is not directly related to swimming for these medusae. Although jet propulsion is effective for rapid body movement, it is energetically costly because the energy expended to accelerate the medusa increases as the square of the medusa's velocity (Ford and Costello, 2000). However, the energetic expense of swimming by these medusae is minimized by the low proportion of time they spend swimming (J. H. Costello, E. Klos and S. P. Colin, unpublished results). In contrast, oblate medusae are often cruising predators and spend the majority of their time swimming (J. H. Costello, E. Klos and S. P. Colin, unpublished results). Viewed in cross section, the wake of an oblate medusa can be visualized as a series of vortices created by alternating contraction and relaxation of the medusan bell (Fig. 7). Viewed in three dimensions, this vortex trail is a pulsed series of vortex rings, or toroids, which pass sequentially down the length of the medusan body, carrying entrained fluid and particles into contact with the oral arms and tentacles trailing in the wake. Flows past the bodies of all the oblate medusae examined here (Fig. 4), as well as oblate medusae documented elsewhere (Larson, 1987; Costello and Colin, 1994, 1995), are characterized by $Re>10^2$. Consequently, inertial forces, which transport the prey entrained in these flows, dominate the flows around these medusan bodies. Therefore, for a number of oblate medusae, bell pulsations create a feeding current that draws prey past the bell margin and into their extended tentacles (Costello and Colin, 1994, 1995). Feeding rates for these cruising medusae are increased by maximizing the volume of fluid transported through the tentacles and the time spent swimming. The oblate bells of these medusae allow the bell margins effectively to act as paddles to push fluid past the bell and into the trailing tentacles. The comparatively high added mass of the oblate bell morphologies allows acceleration of a larger fluid volume to a lower velocity relative to that of prolate forms. Although this rowing motion achieves lower medusan velocities and accelerations, it is energetically less costly and results in higher Froude propulsion efficiencies (Ford and Costello, 2000), which are favorable for a cruising foraging mode (Colin and Costello, 1996).

Considered in isolation from one another, variations in bell morphology, swimming performance, propulsive mechanism or foraging mode appear to confer a range of competitive advantages to various hydromedusae. However, the trade-offs involved in each of these traits become more apparent when they are viewed within the context of suites of co-evolved traits allowing medusae to exploit differing resources within the planktonic environment.

References

Blake, R. W. (1981). Mechanics of drag-based mechanisms of propulsion in aquatic vertebrates. *Symp. Zool. Soc. Lond.* **48**, 29–52.

Bone, Q. and Trueman, E. R. (1982). Jet propulsion of the calyophoran siphonophores *Chelophyes* and *Abylopsis*. *J. Mar. Biol. Ass. UK* **62**, 263–276.

Brusca, R. C. and Brusca, G. J. (1990). *Invertebrates*. Sunderland, MA: Sinaur Associates Inc. 922pp.

Colin, S. P. and Costello, J. H. (1996). Relationship between morphology and hydrodynamics during swimming by the hydromedusae *Aequorea victoria* and *Aglantha digitale*. *Sci. Mar.* **60**, 35–42.

Costello, J. H. (1992). Foraging mode and energetics of hydrozoan medusae. *Sci. Mar.* **56**, 185–191.

Costello, J. H. and Colin, S. P. (1994). Morphology, fluid motion and predation by the scyphomedusa *Aurelia aurita*. *Mar. Biol.* **121**, 327–334.

Costello, J. H. and Colin, S. P. (1995). Flow and feeding by swimming scyphomedusae. *Mar. Biol.* **124**, 399–406.

Costello, J. H., Klos, E. and Ford, M. D. (1998). In situ time budgets of the scyphomedusae *Aurelia aurita*, *Cyama* sp., and *Chrysaora quinquecirrha*. *J. Plankton Res.* **20**, 383–391.

D'Ambra, I., Costello, J. H. and Bentivegna, F. (2002). Flow and prey capture by the scyphomedusa *Phyllorhiza punctata* von Lendenfeld 1884. *Hydrobiologia* (in press).

Daniel, T. L. (1983). Mechanics and energetics of medusan jet propulsion. *Can. J. Zool.* **61**, 1406–1420.

Daniel, T. L. (1984). Unsteady aspects of aquatic locomotion. *Am. Zool.* **24**, 121–134.

Daniel, T. L. (1985). Cost of locomotion: unsteady medusan swimming. *J. Exp. Biol.* **119**, 149–164.

Daniel, T. L. (1995). Invertebrate swimming: integrating internal and external mechanics. In *Biological Fluid Dynamics* (ed. C. P. Ellington and T. J. Pedley), pp. 61–89.

DeMont, M. E. and Gosline, J. M. (1988a). Mechanics of jet propulsion in the hydromedusan jellyfish, *Polyorchis penicillatus*. I. Mechanical properties of the locomotion structure. *J. Exp. Biol.* **134**, 313–332.

DeMont, M. E. and Gosline, J. M. (1988b). Mechanics of jet propulsion in the hydromedusan jellyfish, *Polyorchis penicillatus*. II. Energetics of the jet cycle. *J. Exp. Biol.* **134**, 333–345.

DeMont, M. E. and Gosline, J. M. (1988c). Mechanics of jet propulsion in the hydromedusan jellyfish, *Polyorchis penicillatus*. III. A natural resonating bell, the presence and importance of a resonant phenomenon in the locomotor structure. *J. Exp. Biol.* **134**, 347–361.

Denny, M. W. (1993). *Air and Water: The Biology and Physics of Life's Media*. Princeton, NJ: Princeton University Press. 341pp.

Denton, E. J. and Shaw, T. I. (1961). The buoyancy of gelatinous marine animals. *Proc. Physiol. Soc.* **161**, 14–15.

Donaldson, S., Mackie, G. O. and Roberts, A. O. (1980). Preliminary observations on escape swimming and giant neurons in *Aglantha digitale*. *Can. J. Zool.* **58**, 549–552.

Ford, M. D. and Costello, J. H. (2000). Kinematic comparison of bell contraction by four species of hydromedusae. *Sci. Mar.* **64**, 47–53.

Ford, M. D., Costello, J. H., Heidelberg, K. B. and Purcell, J. E. (1997). Swimming and feeding by the scyphomedusa *Chrysaora quinquecirrha*. *Mar. Biol.* **129**, 355–362.

Gladfelter, W. G. (1972). Structure and function of the locomotory system of the Scyphomedusa *Cyanea capillata*. *Mar. Biol.* **14**, 150–160.

Gladfelter, W. G. (1973). A comparative analysis of the locomotory systems of medusoid Cnidaria. *Helgol. Wiss. Meeresunters.* **25**, 228–272.

Larson, R. J. (1987). Costs of transport for the scyphomedusae *Stomolophus meleagris* L. Agassiz. *Can. J. Zool.* **65**, 2690–2695.

Larson, R. J., Matsumoto, G. I., Madin, L. P. and Lewis, L. M. (1992). Deep-sea benthic and benthopelagic medusae: recent observations from submersibles and a remotely operated vehicle. *Bull. Mar. Sci.* **51**, 277–286.

Lauder, G. V. and Jayne, B. C. (1996). Pectoral fin locomotion in fishes:

Testing drag-based models using three-dimensional kinematics. *Am. Zool.* **36**, 567–581.

Madin, L. P. (1988). Feeding behavior of tentaculate predators: *in situ* observations and a conceptual model. *Bull. Mar. Sci.* **43**, 413–429.

Mills, C. B. (1981a). Diversity of swimming behaviors in hydromedusae as related to feeding and utilization of space. *Mar. Biol.* **64**, 185–189.

Mills, C. B. (1981b). Seasonal occurrence of planktonic medusae and ctenophores in the San Juan Archipelago (NE Pacific). *Wasmann J. Biol.* **39**, 6–29.

Mills, C. B. (1995). Medusae, siphonophores and ctenophores as planktivorous predators in changing global ecosystems. *ICES J. Mar. Sci.* **52**, 575–581.

Strand, S. W. and Hamner, W. M. (1988). Predatory behavior of *Phacellophora camtschatica* and size-selective predation upon *Aurelia aurita* (Scyphozoa: Cnidaria) in Saanich Inlet, British Columbia. *Mar. Biol.* **99**, 409–414.

Vogel, S. (1994). *Life in Moving Fluids: The Physical Biology of Flow.* Princeton, NJ: Princeton University Press. 467pp.